# Stationary Couette flows of elastoviscoplastic fluids are non-unique

Ibrahim Cheddadi, Pierre Saramito, François Graner

# Stationary Couette flows of elastoviscoplastic fluids are non-unique

I. Cheddadi, P. Saramito and F. Graner

**Abstract**

The Herschel-Bulkley rheological fluid model includes viscosity and plasticity. In this classical model, under the yield stress the material is strictly rigid. Complementing this model by including an elastic behavior under the yield stress leads to a description of elastoviscoplastic (EVP) materials such as suspensions or liquid foams. We include this modification in a completely tensorial description of Couette shear flows. Both the parameters of the model, at the scale of a representative volume element, and the predictions (velocity, strain and stress fields), can be readily compared with experiments. We perform a detailed study of the effect of the main parameters, especially the yield strain. We discuss the role of flow lines curvature in the apparition of localisation; we determine the value of the localisation length and provide its approximate analytical expression. We then show that, in our tensorial EVP model of Couette shear flows, normal stresses strongly influence velocity profiles, which can be smooth or non-smooth according to the stress initial conditions. This feature can explain several open debates regarding experimental measurements on Couette flows for various EVP materials such as suspensions or liquid foams, including the non-reproducibility that has been reported in flows of foams. We then discuss the suitability of Couette flows to measure rheological properties of EVP materials.

**Keywords**: elastoviscoplastic / viscoelastoplastic fluids ; non-Newtonian fluids ; Couette experiment ; liquid foam ; suspensions ; mathematical modelling ; numerical simulation.

# Introduction

Localization is a phenomenon often observed in two- or three-dimensional shear flows of complex materials: Coussot et al. (2002) observed it for emulsions, Salmon et al. (2003a) for coloids, and Howell et al. (1999); Mueth et al. (2000); Losert et al. (2000); Huang et al. (2005) for wet granular materials. It consists in a coexistence between a region localized

near a moving boundary, where the material flows like a liquid, and another region where the material is rigid like a solid.

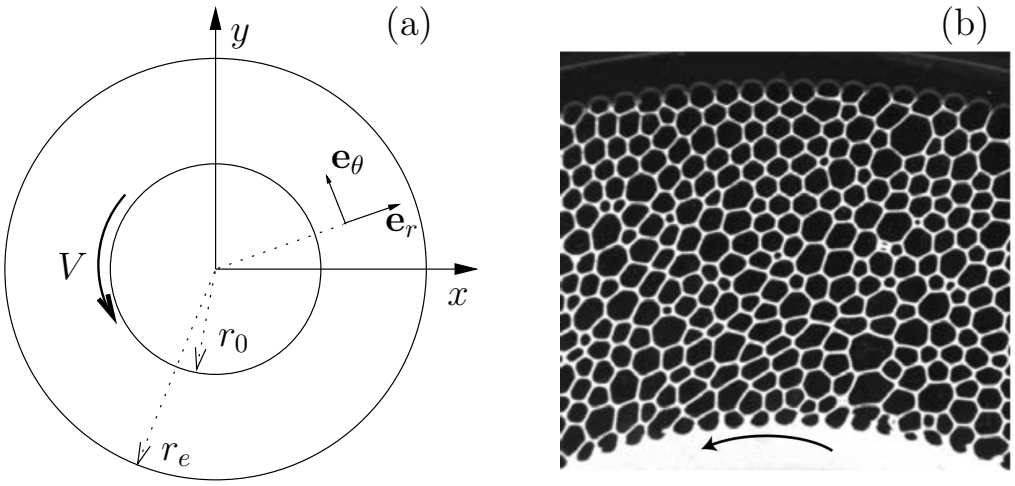


Figure 1: Experimental set-up for a two-dimensional circular shear flow of a foam confined between two horizontal plates. (a) definition of the geometric and kinematic parameters ; (b) picture of the confined bidimensional liquid foam (from Debrégeas et al. (2001)): the internal radius is $r_0 = 71$ mm.

Since the pioneering experiment of Debrégeas et al. (2001) (see Fig. 1), liquid foams (gas bubbles dispersed within a continuous liquid phase, as explained by Weaire and Hutzler (1999); Cantat et al. (2010)) have been widely used to study localization. As a matter of fact, they are suitable for experimental, theoretical and numerical approaches, and direct comparisons between them (for reviews see e.g. Höhler and Cohen-Addad (2005); Schall and van Hecke (2010); Barry et al. (2011)). Their discrete units are the gas bubbles, which are typically millimetric and thus accessible to direct observation. Moreover, they display simultaneous elastic, viscous, plastic behaviors (referred to as *elastoviscoplastic*, or EVP), thus covering a wide range of behaviors observed in many complex materials. Recently, Coussot et al. (2002) used MRI methods to measure local velocity in 3D flows of other EVP materials such as bentonite, carbopol, cement. Despite the apparent simplicity of shear flows, a common description of these experiments is still lacking.

The aim of this paper is to show that including the elasticity in the classical viscoplastic Herschel-Bulkley (VP) model in a simple manner leads to many improvements in the understanding of Couette flows of various complex fluids, such as suspensions, emulsions or liquid foams. Cheddadi et al. (2008, 2009, 2011a) have previously explored this approach for Couette flows of liquid foams and complex flows around an obstacle ; they have explained the observations of normal stresses components measured by Janiaud and Graner (2005) in experimental data by Debrégeas et al. (2001); Kabla (2003), that are not captured by

non-tensorial (scalar) models.

In the present work, the theoretical predictions are compared with experimental measurements, including shear and normal stresses when available. We propose an in-depth study of the influence of the dimensionless rheological parameters, including the influence of the Couette geometry confinement (see table 1). For simplicity, we focus here on the low velocity regime corresponding to most published foam Couette flow experiments, and keep for a future work the high velocity regime where viscous and friction effects are dominant (see e.g. Katgert et al. (2008, 2009, 2010)). Being tensorial and EVP are two essential features of the present modelling, leading to three predictions not captured by scalar and/or VP models. First, we show that tensorial stresses that depend on the preparation of the material can persist as residues even in the stationnary flow. Second, depending on shear and normal stresses, velocity flow profiles are either smooth or non-smooth. Third, as a consequence of both preceding results, Couette flows of EVP materials are non-unique, even in stationary regime.

The outline of the paper is as follows. Section 1 reviews and discusses the main open questions found in the literature, which we want to address here. Section 2 presents the mathematical equations introduced by Saramito (2007, 2009), their solutions (Fig. 2) and some of their main features completely absent from the VP model: effect of initial conditions, memory effect, non-uniqueness, non-smooth solutions; it also explains how the model can be compared to actual experimental data (section 2.3). Section 3 examines how variations of the parameters of the model affect these flow features, and provides an approximate analytical expression for the localisation length (eq. 6). Section 4 is devoted to a discussion and some perspectives of both experimental and numerical modelling of foam flows.

| symbol | name | definition | physical meaning | typical range |
|---|---|---|---|---|
| $\varepsilon_Y$ | yield strain | $\dfrac{\tau_Y}{2\mu}$ | elastoplasticity | $[0, 0.5]$ |
| $Bi$ | Bingham | $\dfrac{\tau_Y \Delta r}{\eta V}$ | viscoplasticity | $[0, 100]$ |
| $Co$ | confinement | $\dfrac{r_e - r_0}{r_e}$ | curvature | $]0, 1[$ |
| $n$ | power index | | shear thinning | $[0.3, 1]$ |
| $We$ | Weissenberg | $\dfrac{\eta V}{\mu \Delta r} = \dfrac{2\varepsilon_Y}{Bi}$ | viscoelasticity | $[0, 0.04]$ |

Table 1: Four dimensionless numbers $(\varepsilon_Y, Bi, Co, n)$, or equivalently $(We, Bi, Co, n)$, which completely characterize the problem.

# 1 Open questions

During the last ten years the literature has debated on the Couette flow of various complex fluids, raising some theoretical questions (see eg. Schall and van Hecke (2010)):

- What is the physical origin of localization ?
- What is the position of the localization, defined as the position separating the flowing region from the rigid one ?
- Why, at the transition between these regions, do some experiments report smooth profiles and some others experiments report non-smooth ones ?

Before we examine the status of these questions, we first need to clarify the vocabulary used in the literature. When comparing different articles, it is necessary to keep in mind that the position of the localization, denoted as $r_c$, admits several possible definitions (see section 7.3 of Weaire et al. (2010)). Gilbreth et al. (2006) explored also several ways to define $r_c$ are investigated. Similarly, there are at least two different ways used to define the norm of a tensor, and thus the von Mises criterion and the yield strain and stress (see eq. 2 and discussion thereafter). Moreover, since the words "shear banding" are used according to different definitions, we prefer not to use them. Finally, we assume here that the materials can be described using continuum mechanics: this implies that there is a representative volume element (RVE), smaller than the global flow, but large enough so that one can define variables such as stresses, strains, velocity gradient, and parameters, such as elastic modulus, yield strain and viscosity.

## 1.1 What is the physical origin of the localization ?

There are several explanations for the origin of the localization; many of them are reviewed and discussed by Schall and van Hecke (2010).

**Explanations invoking a non-monotonous constitutive equation**.

In complex materials which display a shear-induced structural transition, the coexistence of two different shear rates with the same stress, that is, if the shear stress versus *shear rate* curve is *multi-valued*, see work by Berret et al. (1994); Porte et al. (1997); Decruppe et al. (2001), is a possible source of localization. Alternatively, foams experiments led by Khan et al. (1988) and simulations led by Kabla et al. (2007); Okuzono and Kawasaki (1995); Raufaste et al. (2010), suggest that in the quasi-static regime the shear stress versus *shear strain* curve passes through an *overshoot* before reaching a plateau, thus being multi-valued: Clancy et al. (2006); Weaire et al. (2010) also suggest this as a possible cause of localization.

We question the fact that this explanation could be general for foams involved in Couette experiments: they usually contain at least a few percents of liquid, so that their yield strain is lower (see Marmottant et al. (2008)) and the overshoot becomes impossible to observe (see Raufaste et al. (2010)). Moreover, even in theory and simulations of dry foams, the overshoot disappears if the foam is too disordered (see Raufaste et al. (2010)). Discussing that point is beyond the scope of the present paper, where we explore the complex behavior emerging from a simple EVP constitutive equation.

**Explanations invoking a non-homogeneous $\sigma$.** This mechanism arises in rheological models that include a yield stress, like the VP model or the elastoviscoplastic (EVP) model by Saramito (2007): in the case of a circular Couette geometry, the curvature induces a spatial heterogeneity of the stress, the inner part being above the yield stress and flowing, and the outer part being under the yield stress and non-flowing.

An alternative interpretation has been presented by Wang et al. (2006) for bidimensional foams; they performed experiments with two configurations in a *plane* Couette geometry: either bubbles floating on water (bubble raft), or bubbles confined between water and a glass plate. They observed localization only in the first case, when glass plates are present. Therefore, the competition between the internal viscosity of the foam and the *external friction* from the glass plates has been suggested by Janiaud et al. (2006) as a possible cause for localization, even in the case of circular geometries (see Clancy et al. (2006)).

Cheddadi et al. (2008) have reconciled these views by performing a detailed comparison of the Saramito (2007) EVP model with both stationary and transient regimes of the Debrégeas et al. (2001) experiment of a bidimensional foam confined between two glass plates. They have showed that the simple explanation of a non-homogeneous stress is still valid for such systems. The curvature of flow lines and the friction on the glass plates are only two different possible causes for stress heterogeneity.

In practice, we have also shown that the friction of glass plates is so small that is plays a visible role only in the absence of flow line curvature, as in the plane geometry of Wang et al. (2006). In cylindrical Couette flows, the available data are not compatible with this friction-dominated interpretation, and are compatible with the stress heterogeneity that arises from geometry. In what follows, we neglect the friction on plates, and use bidimensional foams as model systems for other complex fluids.

## 1.2 What is the position of the localization $r_c$ ?

Weaire et al. (2010) have reviewed the current knowledge of the dependency of the position of the localization with the cylinder velocity. They find that in the low velocity regime, it is basically undetermined: there is a range of possible values for the position of the localization and, moreover, the size of this range diverges when the velocity decreases. There is thus a

double question: is there a hidden variable which fixes the position of localization ? for a given experiment, is the position predictable ?

To answer this double question, we explicitly determine the position of localization and study its dependence with initial conditions.

## 1.3 Why smooth and/or non-smooth profiles ?

The first observation of foam Couette flows by Debrégeas et al. (2001) reported a *smooth* velocity profile (Fig. 3a).

However, in 2002, Coussot et al. (2002); da Cruz et al. (2002) rather observed *discontinuous* shear rate profiles on Couette flows of emulsions and suspensions (Fig. 3b). A discontinuity of the shear rate, denoted as $\dot{\gamma}_c$ at $r = r_c$, was measured: in that case, the velocity profile is non-smooth at $r = r_c$, since its derivative is related to the shear rate. Such non-smooth profiles were confirmed until 2008 for various slurries and pastes by Huang et al. (2005), for worm-like micelles by Salmon et al. (2003a), for lyotropic lamellar systems by Salmon et al. (2003b), for Couette foam flows by Lauridsen et al. (2004); Gilbreth et al. (2006); Dennin (2008); Krishan and Dennin (2008), and interpreted theoretically by Denkov et al. (2009); Clancy et al. (2006); Weaire et al. (2010).

Surprisingly, experiments were published by Katgert et al. (2008, 2009, 2010); Coussot and Ovarlez (2010); Ovarlez et al. (2010)in 2008-2010, reverting to smooth velocity profiles at $r = r_c$, and continuous shear rates ($\dot{\gamma}_c = 0$). This of course stirred a controversy, fuelled by the facts that some papers with strictly opposed results shared either an author, P. Coussot, in Coussot et al. (2002); da Cruz et al. (2002); Huang et al. (2005); Coussot and Ovarlez (2010) or a set-up, the bubble raft, in Lauridsen et al. (2004); Gilbreth et al. (2006); Dennin (2008); Krishan and Dennin (2008); Katgert et al. (2008, 2009, 2010).

The tendency was thus to question the quality of the experiments. Coussot and Ovarlez (2010) explained this discrepancy between his own measurements as: "*previous data on a specific foam (Rodts et al. (2005)) were probably affected by experimental artefacts*". Similarly, Ovarlez et al. (2010) explain that "*Our measurements demonstrate that three-dimensional foams do not exhibit observable signatures of* [discontinuous] *shear banding. This contrasts with the results of Rodts et al. (2005) and da Cruz et al. (2002) which we have shown to pose several experimental problems*" and have to mention that "*the case of bubble rafts is still unclear*".

Our theoretical approach is an attempt to reconcile these measurements by finding a deeper reason to explain why, in some case, either a smooth or a non-smooth profile could appear. We point out the influence of the stress initial conditions. This could rehabilitate the quality of the published data and rather point to the sensibility of the equations.

# 2 Modelling

## 2.1 Equations

In 1926, Herschel and Bulkley (1926) proposed a power law variant of the viscoplastic Bingham model ( Bingham (1922); Oldroyd (1947)):

$$\begin{cases} \tau = 2K|D|^{n-1}D + \tau_Y \dfrac{D}{|D|} & \text{when } |D| \neq 0 \\ |\tau_d| \leq \tau_Y & \text{otherwise} \end{cases} \iff \max\left(0,\ \frac{|\tau_d| - \tau_Y}{2K|\tau|^n}\right)^{\frac{1}{n}} \tau = D \quad (1)$$

where $\tau$ is the stress tensor, $D = (\nabla \mathbf{v} + \nabla \mathbf{v}^T)/2$ is the rate of deformation tensor, $\mathbf{v}$ is the velocity, and $\nabla \mathbf{v} = (\partial_j v_i)$ is the velocity gradient. Here, $\tau_Y > 0$ the yield stress, $K > 0$ the consistency parameter, and $n > 0$ is the power index. When $n = 1$ the model reduces to the Bingham model. The shear thinning behavior is associated with $0 < n < 1$ and the unusual shear thickening behavior to $n > 1$.

The von Mises criterion $|\tau_d| \geq \tau_Y$ involves the matrix norm of the deviatoric part of the stress. In cylindrical coordinates it writes:

$$|\tau_d| = \left(2\tau_{r\theta}^2 + \frac{(\tau_{rr} - \tau_{\theta\theta})^2}{2}\right)^{\frac{1}{2}} \quad (2)$$

Note that, favoring the shear stress, some authors uses a slightly different definition of the norm: $(\tau_{r\theta}^2 + (\tau_{rr} - \tau_{\theta\theta})^2/4)^{\frac{1}{2}}$. This alternative definition leads to an equivalent model: it only changes by a $1/\sqrt{2}$ factor the yield stress $\tau_Y$ and by a power of two factor the consistency $K$.

The VP model predicts localization in the circular Couette geometry, as a result of the stress heterogeneity. Its position $r_c$ can be easily computed from a simple expression (see appendix B, equation (12)).

For the Couette problem, $V$ denotes the velocity of the inner cylinder and $\Delta r = r_e - r_0$ the width of the gap. Note that $\eta = K(V/\Delta r)^{n-1}$ has the dimension of a viscosity, The dimensionless Bingham number is:

$$Bi = \frac{\tau_Y \Delta r}{\eta V}$$

It compares the yield stress $\tau_Y$ with a characteristic viscous stress $\eta V/\Delta r$. Let us also introduce the confinement dimensionless number

$$Co = 1 - \frac{r_0}{r_e},$$

that expresses the eccentricity of the Couette geometry: when the two radii are close, this number is close to zero. Conversely, when the eccentricity is extreme, e.g. $r_0$ becomes small, this number tends to one.

Saramito (2007, 2009) derived a three-dimensional combination elastoviscoplastic (EVP) of the viscoelastic (VE) Oldroyd and viscoplastic (VP) Herschel-Bulkley model:

$$\frac{1}{2\mu} \overset{\nabla}{\tau} + \max\left(0,\ \frac{|\tau| - \tau_Y}{2K|\tau|^n}\right)^{\frac{1}{n}} \tau = D \tag{3}$$

where $\mu > 0$ is the elasticity modulus. When $1/\mu = 0$ we obtain the VP model. Conversely, when $n = 1$ and $\tau_Y = 0$ we obtain the Oldroyd viscoelastic model (Oldroyd (1950)). The so-called upper-convected tensorial derivative $\overset{\nabla}{\tau}$ is defined by:

$$\overset{\nabla}{\tau} = \frac{\partial \tau}{\partial t} + \mathbf{v}.\nabla\tau - \tau\nabla\mathbf{v}^T - \nabla\mathbf{v}\tau \tag{4}$$

In addition to the dimensionless numbers $(Bi, Co, n)$ already introduced for the VP model, we define the elastic yield strain $\varepsilon_Y$ as

$$\varepsilon_Y = \frac{\tau_Y}{2\mu}.$$

This dimensionless parameter is a measure of the softness and deformability of the material, it has been evidenced as the main parameter for the characterization of EVP materials by Cheddadi et al. (2011a). In the case of foams, it is directly measurable from experiments (Marmottant et al. (2008)). The elastic properties of the material can also be parameterized by the Weissenberg number $We$ that compares the characteristic viscous stress $\eta V/\Delta r$ with the elastic modulus $\mu$; it allows to make the link with VE models such as Oldroyd one. Finally, the problem is completely characterized by four dimensionless numbers (see table 1): namely $(\varepsilon_Y, Bi, Co, n)$, or equivalently, $(We, Bi, Co, n)$.

## 2.2 Overview of EVP solutions for Couette flows

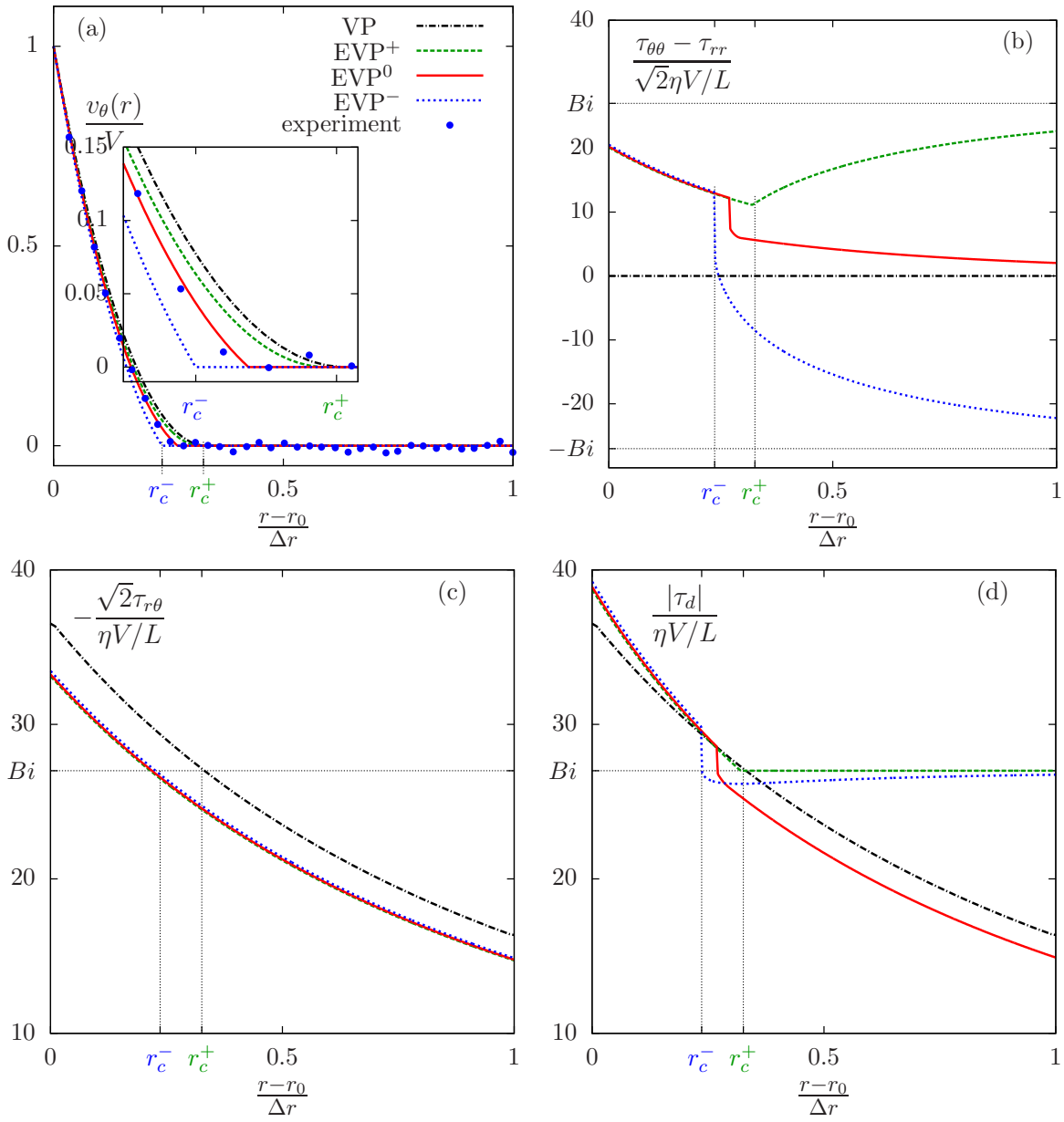


Figure 2: Comparison EVP/VP, stationary solution: (a) velocity, (b) normal stress, (c) shear stress, (d) norm of the deviatoric stress. EVP solutions for the reference set of parameters (eqn (5) and Fig. 3b): $\varepsilon_Y = 0.35$, $Bi = 27$, $Co = 1/3$, $n = 1$, as on Fig. 3b, with different initial conditions. Thick solid red line (denoted as EVP$^0$): $\tau^0_{\theta\theta} = 0$; thin dashed black line (EVP$^+$): $\tau^0_{\theta\theta} = \sqrt{2}Bi$; thin dotted blue line (EVP$^-$): $\tau^0_{\theta\theta} = -\sqrt{2}Bi$; thick solid green line (VP): $Co = 1/3$, $Bi = 27$, $n = 1$. We denote as $r_c^+$ (resp. $r_c^-$) the critical radius of solution EVP$^+$ (resp. EVP$^-$).

We now review some of the specificities brought by the tensorial EVP model, with an emphasis on the differences with scalar VP models. Fig. 2 shows all the components of some solutions of the EVP model, for a set of parameters used as reference (eqn (5) and Fig. 3b), and compares them to the Herschel-Bulkley VP model. The exploration of these parameters in a much larger range will be presented in section 3.

**Range of possible initial conditions**. The EVP constitutive equation (3) includes derivatives with respect to time of the elastic stress tensor and therefore allows the study of transient flows, as has been done by Cheddadi et al. (2008). This in turn requires to specify an initial condition that reflects the preparation of the material before the beginning of the experiment. In particular, the tensorial frameworks allows to study various initial normal stresses.

Three different constant values for $\tau_{\theta\theta}$ are chosen. We note EVP$^0$ the case without initial normal stress, $\tau_{\theta\theta}(t=0)=0$. We then explore two extreme limit cases, such that the norm of the initial deviatoric stress tensor is $|\tau_d(t=0)|=\tau_Y$, while other stress components are zero $\tau_{r\theta}(t=0)=\tau_{rr}(t=0)$. We thus introduce the two cases EVP$^{\pm}$ corresponding to initial stresses $\tau_{\theta\theta}(t=0)=\pm\sqrt{2}\tau_Y$. We denote as $r_c^+$ (resp. $r_c^-$) the extreme critical radius, corresponding to EVP$^+$ (resp. EVP$^-$).

**Effect of the initial conditions**.

Surprisingly, Fig. 2 shows that the stationary solution depends on the initial conditions. We find that they lead to three different stationary solutions, both for the velocity profile (Fig. 2a) and for the stress (Fig. 2b-d). For a given set of parameters $(\varepsilon_Y, Bi, Co, n)$, when the initial condition varies the model predicts a *continuous set of stationary solutions*. Depending on the initial condition, the critical radius $r_c$ can reach any value in the range $[r_c^-, r_c^+]$; the highest critical shear rate is reached for the solution with $\tau_{\theta\theta}(t=0)=-\sqrt{2}\tau_Y$.

**Non-uniqueness**. Here, we find that $r_c^+=2.33\Delta r$ is close to the value predicted by the VP model, but $r_c^-=2.24\Delta r$ is significantly smaller, while the critical radius $r_c^0=2.28$ for EVP$^0$ is in between. The EVP model contrasts dramatically with the the VP one, where the (stationary) velocity is unique, the normal stress components are zero and the localization length $r_c$ is also unique.

**Memory effects**. Unlike the VP model, the EVP model exhibits non-zero normal stresses (Fig. 2b): in the flowing region ($r<r_c$) where plastic rearrangement continuously occur ($|\tau_d|>\tau_Y$), the normal stress is independent of the initial condition, the material loses progressively memory of the initial condition. Conversely, in the non-flowing region ($r>r_c$ and $|\tau_d|<\tau_Y$), the normal stress highly depends on the initial conditions. The material thus keeps track of the initial condition through residual normal stresses.

**Smooth and non-smooth solutions**.

Unlike the VP model, EVP solutions can exhibit either smooth ($EVP^+$), or non-smooth profiles ($EVP^0$, $EVP^-$): the velocity gradient and the normal stress can be discontinuous at $r = r_c$ (Fig. 2a). We define the critical shear rate $\dot{\gamma}_c$ as the jump of $\dot{\gamma} = 2D_{r\theta}$ at $r = r_c$, it is directly related to the slope of the velocity (Fig. 2a). Compared to $EVP^0$, $EVP^-$ exhibits a stronger localization ($r_c^- < r_c^0$), a higher $\dot{\gamma}_c$, and a higher jump of the normal stress (Fig. 2.c).

**Comment on the non-uniqueness**.

Let us analyze the source of the non-uniqueness of the solution. The VP model (1) contains one non-linearity, related to the von Mises criteria. The EVP model (eq. (3)) adds a second nonlinearity contained in the Oldroyd derivative (eq. (4)). Due to the expression of this Oldroyd derivative, the stationary EVP equations do not reduce to the VP model. The additional term couples the normal stresses components with the shear stress and the velocity gradient (see appendix A). Therefore, even though the velocity gradient reduces here to the shear component, the EVP stationary solution develops non-zero normal stresses.

This additional nonlinearity, interacting with the von Mises criteria, causes non-uniqueness of the stresses at the vicinity of $|\tau_d| = Bi$, i.e. at the vicinity of $r = r_c$.

Of course, *for each given initial condition*, the corresponding time-dependent problem is well-posed, its time-dependent solution is unique, and the associated stationary solution is unique too.

## 2.3 Comparison with experiments: parameters identification

We explain here how the parameters of the model were chosen in order to fit the experimental data shown in Fig. 3.

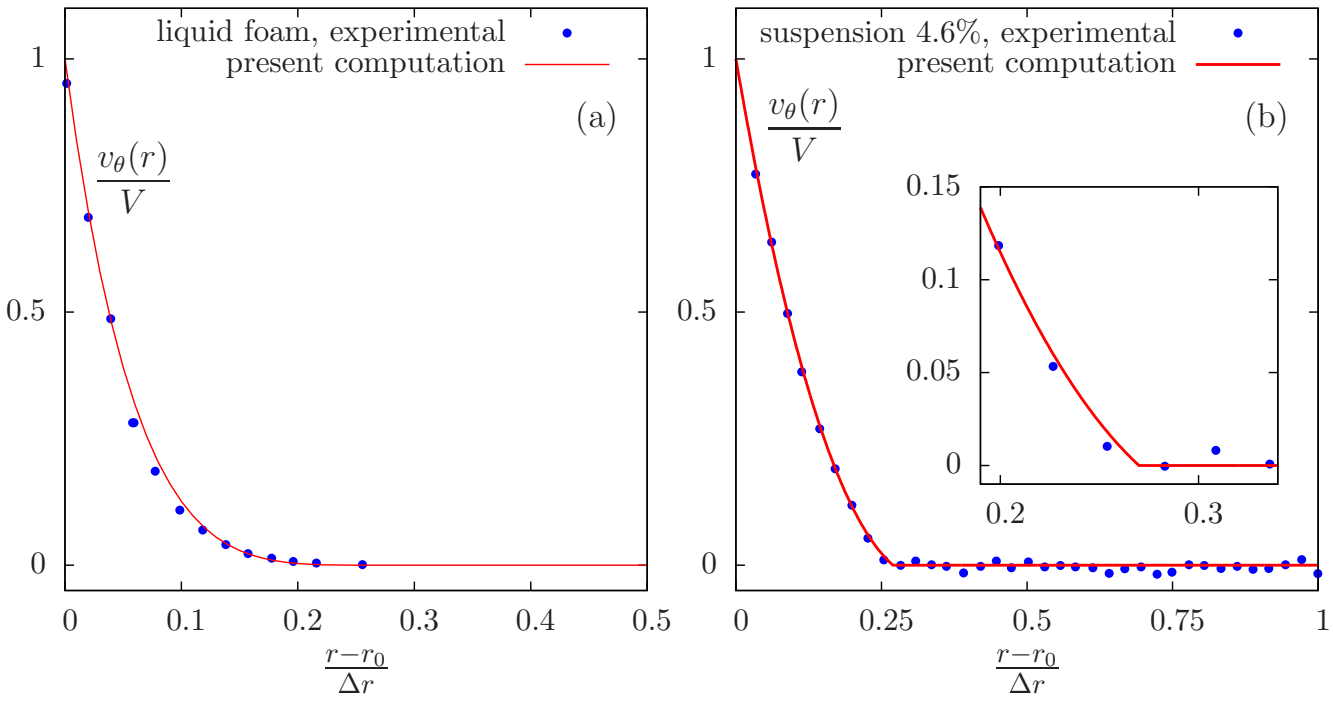


Figure 3: Smooth and non-smooth velocity profiles. Experimental data are compared with our model as discussed in section 2.3. (a) Smooth profile: comparison of experimental data on a foam by Debrégeas et al. (2001) with the present theory ($\varepsilon_Y = 0.175$, $Bi = 10$, $Co = 0.41803$, $n = 1/3$); (b) Non-smooth profile: comparison of experimental data on a bentonite-water suspension from Fig.1.a of Coussot et al. (2002), with the present theory ($\varepsilon_Y = 0.35$, $Bi = 27$, $Co = 1/3$, $n = 1$). Inset: zoom around $r = r_c$.

**Smooth profiles: the Debrégeas experiment**

The first experiment was made with foam by Debrégeas et al. (2001) who measured with image analysis technique the stationary velocity profiles; it was reanalyzed in 2005 by Janiaud and Graner (2005); in particular, they measured the shear and normal components of the local elastic strain, in the transient and stationary regime.

In the experiment, a stationary state is reached after a transient regime. The rotation direction is then inverted, and after a new transient a new stationary state is reached: this is when measurements are recorded (Debrégeas et al. (2001)). To perform a significant comparison, we use the experimental stationary state as an initial condition, invert the rotation, compute the numerical solution until a first stationary state is reached, then invert again the rotation, and compare the corresponding stationary state with experiments.

The confinement number is given by the geometry:

$$Co = 1 - r_0/r_e = 1 - 71/122 \approx 0.41803.$$

We have to adjust the value of the four remaining parameters: $\varepsilon_Y$, $Bi$, $n$. We focus on the stationary measurements of elastic strain and velocity.

We start with the yield strain $\varepsilon_Y$; this parameter is independent of the velocity and exerts a large effect on the elastic strain $\varepsilon^e = \tau_{r\theta}/(2\mu)$ (see Cheddadi et al. (2011b)). We find that $\varepsilon_Y = 0.175$ allows a good fit of the measured value of the shear elastic strain (see Fig. 4a). As a result, the initial normal components of the strain are not affected (see Fig. 4b) by the successive rotations in the region $r > r_c$, that remains under the yield strain $\varepsilon_Y$: this region undergoes reversible elastic deformations.

Then we have to adjust the value of $Bi$ and $n$. These parameters have much less effect on the profiles of $\varepsilon^e$ than $\varepsilon_Y$, but they affect more the localization length and the smoothness of the solution (see Cheddadi et al. (2011b)). As this experiment exhibits a very smooth transition from flowing to non-flowing region (exponential-like decrease of the velocity), it seems relevant from our sensibility analysis (see below, section 3.4) to use a rather small value of the shear-thinning index $n$: we choose the value $n = 1/3$. The localization length can be measured from the experiment: $r_c - r_0 \approx 0.3\ \Delta r$; we can use this information in the EVP model, taking advantage of the fact that the localization is a VP effect and is mostly determined by the underlying Herschel-Bulkley model. This last model yields a relation between the values of $r_c$, $Bi$, and $n$ (see appendix B, equation (12)): with the chosen value of $Co$ and $n = 1/3$, it yields $Bi \approx 7.6$. This value is slightly adjusted in the EVP model: we obtain a better fit of the velocity profile with $Bi = 10$.

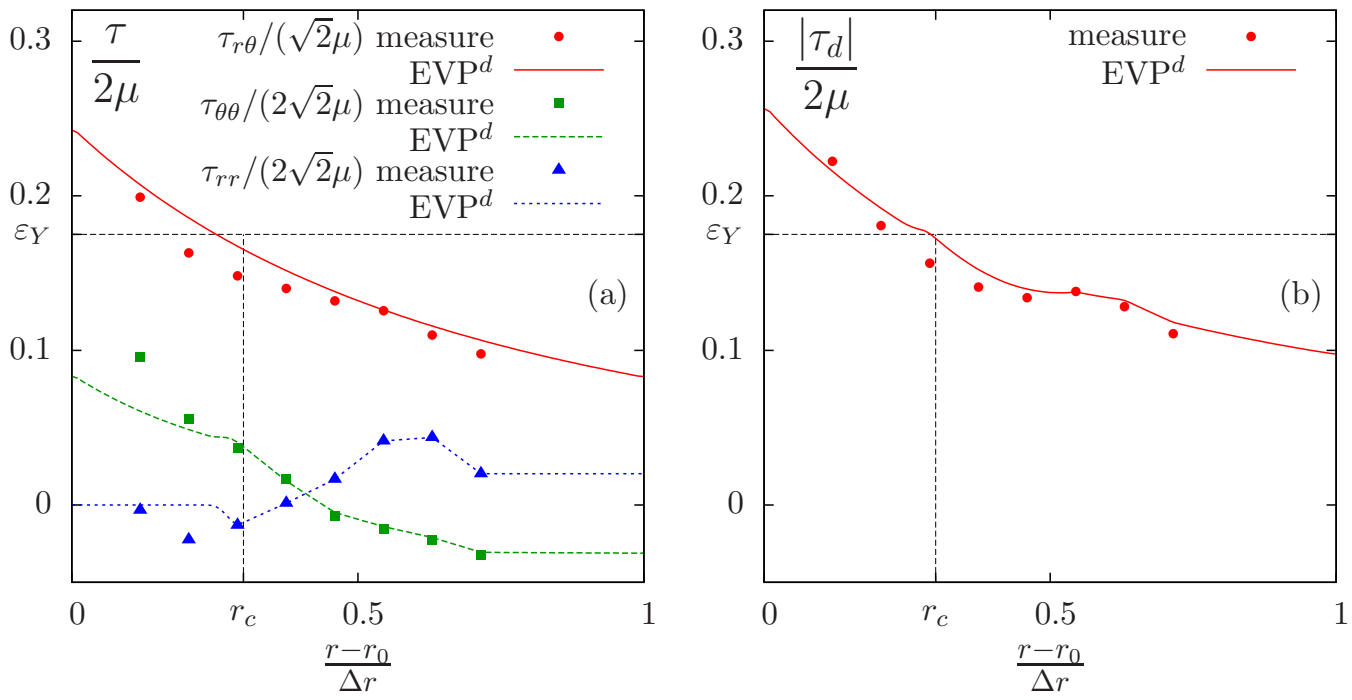


Figure 4: The stress tensor: comparison of experimental measurements (Janiaud and Graner, 2005), as analyzed from (Debrégeas et al., 2001), with computations ($\varepsilon_Y = 0.175$, $Bi = 10$, $Co = 0.41803$, $n = 1/3$); (a) components; (b) norm of the tensor.

**Non-smooth profiles: the Coussot experiment**

The second experiment was made with a bentonite-water suspension by Coussot et al., using MRI (Coussot et al., 2002). For this experiment, only the stationary velocity has been measured, which makes more difficult to precisely evaluate the parameters of the model. Since the normal stresses are not measured, we take an initial condition set to zero for the sake of simplicity. As the velocity profile is quite abrupt at the vicinity of $r = r_c$, we choose $n = 1$ for the shear-thinning index. Then, as for the previous experiment, we evaluate the Bingham number $Bi$ such that the critical radius predicted by underlying Herschel-Bulkley model matches the one of the experiment ($r_c - r_0 = 0.28\ \Delta r$). From this point, the slope of velocity at $r = r_c$ (which is directly related to the critical shear rate) can be adjusted through the yield strain $\varepsilon_Y$. The best fit is obtained with $\varepsilon_Y = 0.35$ and $Bi = 27$.

# 3 Sensitivity to the parameters

Now, we study how the range $[r_c^-, r_c^+]$ and the critical shear rate $\dot{\gamma}_c$ depend on the parameters of the model. We explore the parameters space with the dimensionless numbers $(\varepsilon_Y, Bi, Co, n)$; it allows to probe the effect of the imposed velocity $V$ (through the Bingham number, as it is the only one that depends on $V$); the geometry (through the confinement number $Co$); and two material parameters, the yield strain $\varepsilon_Y$, and the shear thinning index $n$. These parameters are varied around a reference set of parameters used for the comparison with (Coussot et al., 2002) (section 2.3, Fig. 3b):

$$\varepsilon_Y = 0.35, \quad Bi = 27, \quad n = 1, \quad Co = 1/3. \tag{5}$$

## 3.1 Effect of the velocity

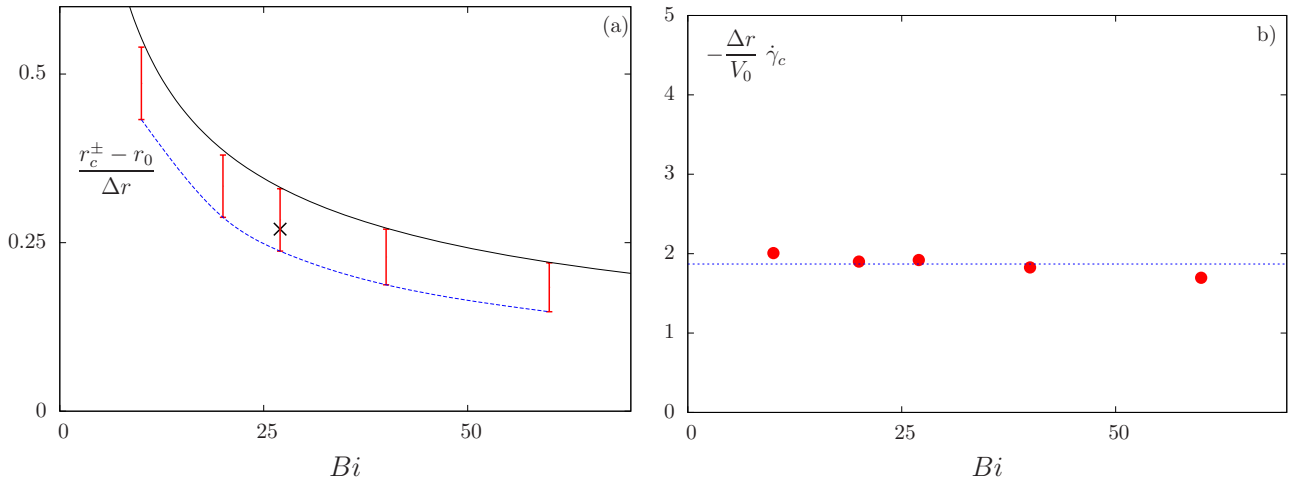


Figure 5: Effect of the viscoplasticity $Bi$: (a) upon $r_c^-$ and $r_c^+$ ; (b) upon $\dot{\gamma}_c$. The solid black line is the value predicted by the Herschel-Bulkley model with the same parameters except that $\varepsilon_Y = 0$. Black cross: parameters as (5) together with $\tau(t=0) = 0$.

The effect of the imposed velocity $V$ is probed through the Bingham number $Bi = \frac{\tau_Y}{\eta V/L}$ that is varied in the range $[10, 60]$, around the reference value $Bi = 27$. If $V_0$ is the velocity associated to this reference value, the range of $Bi$ corresponds roughly to the range $[V_0/3, V_0 \times 3]$ for the velocity. Observe on Fig. 5a that, when the Bingham number $Bi$ increases, $r_c$ decreases and the size of the zero velocity zone increases. The critical radius $r_c^+$ almost matches the critical radius predicted by the Herschel-Bulkley model. The flow becomes more localized and the gap between $r_c^-$ and $r_c^+$ also decreases slowly. The marker represents our reference solution (on Fig. 5a). We observe on Fig. 5b that $\dot{\gamma}_c$ is almost constant when $Bi$ varies.

Varying the velocity affects the size of the zero velocity zone, but has few effects upon the possible abruptness of the solution, nor on the range $[r_c^-, r_c^+]$.

## 3.2 Effect of the confinement $Co$

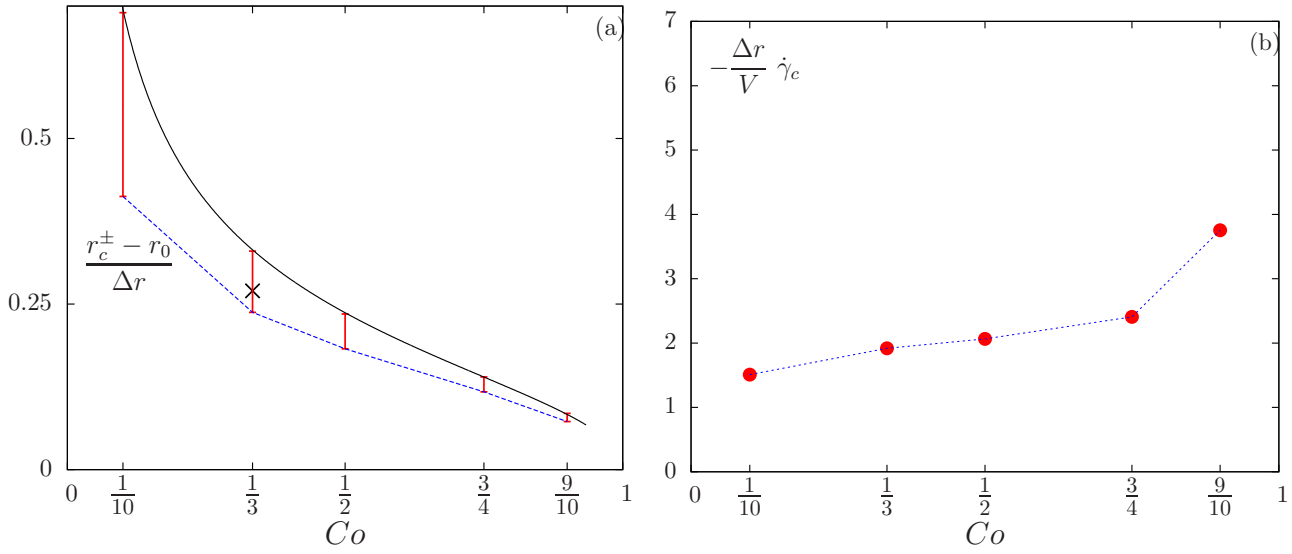


Figure 6: Effect of the confinement $Co$: same caption as Fig. 5.

The Couette number $Co$ explores the effect of the geometry confinement. Recall that $Co \to 0$ corresponds to the plane Couette, with an homogeneous stress throughout the gap, while $Co$ close to one corresponds to an eccentric cylindrical Couette, with an highly heterogeneous stress. Observe on Fig. 6 that the size of the zero velocity zone decreases when $Co$ tends to one. The critical radius $r_c^+$ of the smooth solution is well predicted by the Herschel-Bulkley model. Note also that the difference $r_c^+ - r_c^-$ decreases with $Co$: thus, when the flow is highly localized, the effect of the initial condition is less visible on the localization length. Also the maximal discontinuity $\dot{\gamma}_c$ of the critical shear rate slightly increases with $Co$.

## 3.3 Effect of the elastoplasticity $\varepsilon_Y$

The yield deformation $\varepsilon_Y$ has a large effect on the velocity profile of the extreme non-smooth solution and few impact on the smooth one: $r_c^-$ decreases and $\dot{\gamma}_c$ increases, both quasi-linearly, when $\varepsilon_Y$ increases. A linear regression leads to:

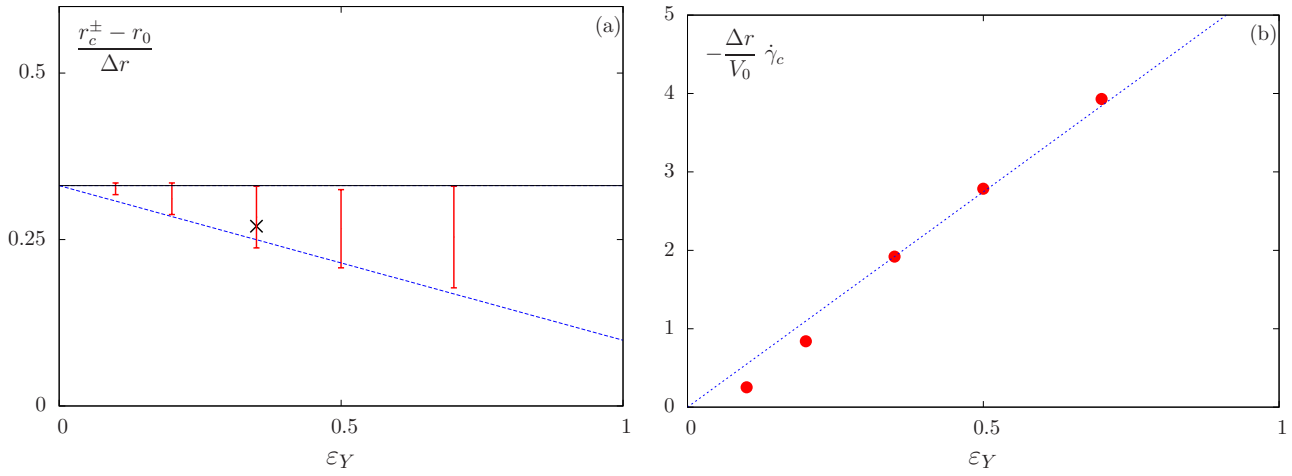


Figure 7: Effect of the elastoplasticity $\varepsilon_Y$: same caption as Fig. 5.

$$\begin{aligned} \frac{r_c^-}{\Delta r} &\approx -0.23\,\varepsilon_Y + 0.33 \\ -\frac{V}{\Delta r}\dot{\gamma}_c &\approx 5.5\,\varepsilon_Y. \end{aligned} \tag{6}$$

Note that both the range $r_c^+ - r_c^-$ and the discontinuity $\dot{\gamma}_c$ increases with $\varepsilon_Y$. Conversely, when $\varepsilon_Y$ vanishes, $r_c^- = r_c^-$ and $\dot{\gamma}_c = 0$: the solution is unique and smooth: there is no more elasticity and the model reduces to the VP one.

## 3.4 Effect of the shear thinning $n$

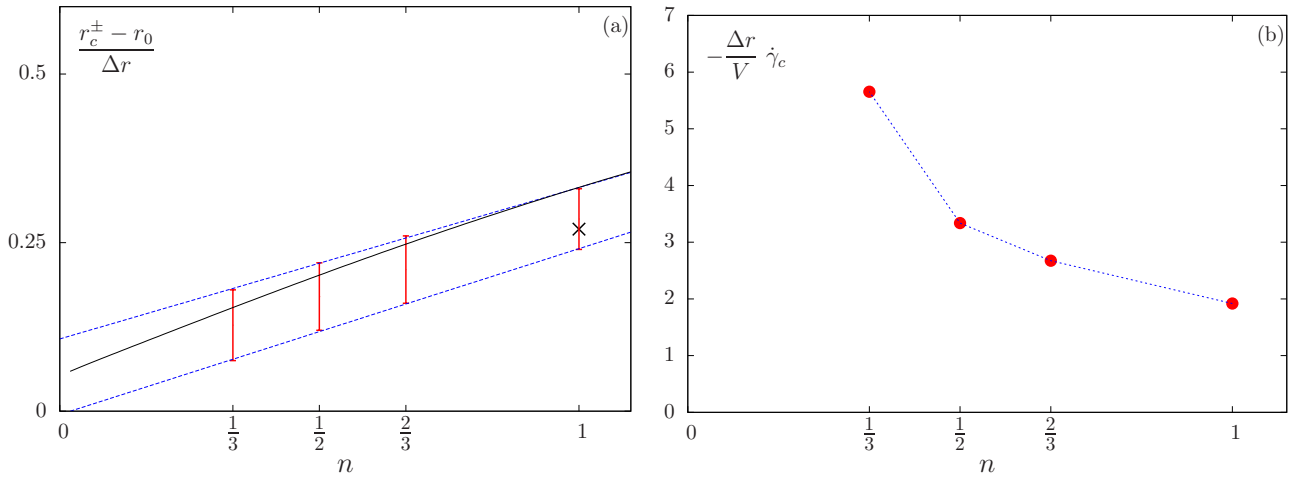


Figure 8: Effect of $n$: same caption as Fig. 5.

From Fig. 8, the solution range $r_c^+ - r_c^-$ appears to be roughly constant while the size of the yielded zone increases with $n$. The critical radius $r_c^+$ decreases with $n$, as for the Herschel-Bulkley model. The $\dot{\gamma}_c$ discontinuity of the shear rate for the extreme non-smooth solution decreases with $n$. These effects are not intuitive: another way to explore the effect of $n$ is to vary it while $r_c$ is held fixed. It can be approximatly achieved with the following procedure that takes advantage of the fact that the critical radius $r_c$ is roughly given by the Herschel-Bulkley model: it allows to predict $r_c$ as a function $Bi$, $n$, $Co$; conversely, for given values of $r_c$, $n$, $Co$, one obtains a unique value of $Bi$; this value is then used in the EVP model.

| $n$ | 1 | 2/3 | 1/2 | 1/3 |
|---|---|---|---|---|
| $Bi$ | 27 | 16.6489 | 12.7851 | 9.54785 |

Table 2: Effect of the shear thinning index $n$ while $r_c$ remains fixed: values of $n$ and corresponding values of $Bi$ ($\varepsilon_Y = 0.35$, $Co = 1/3$).

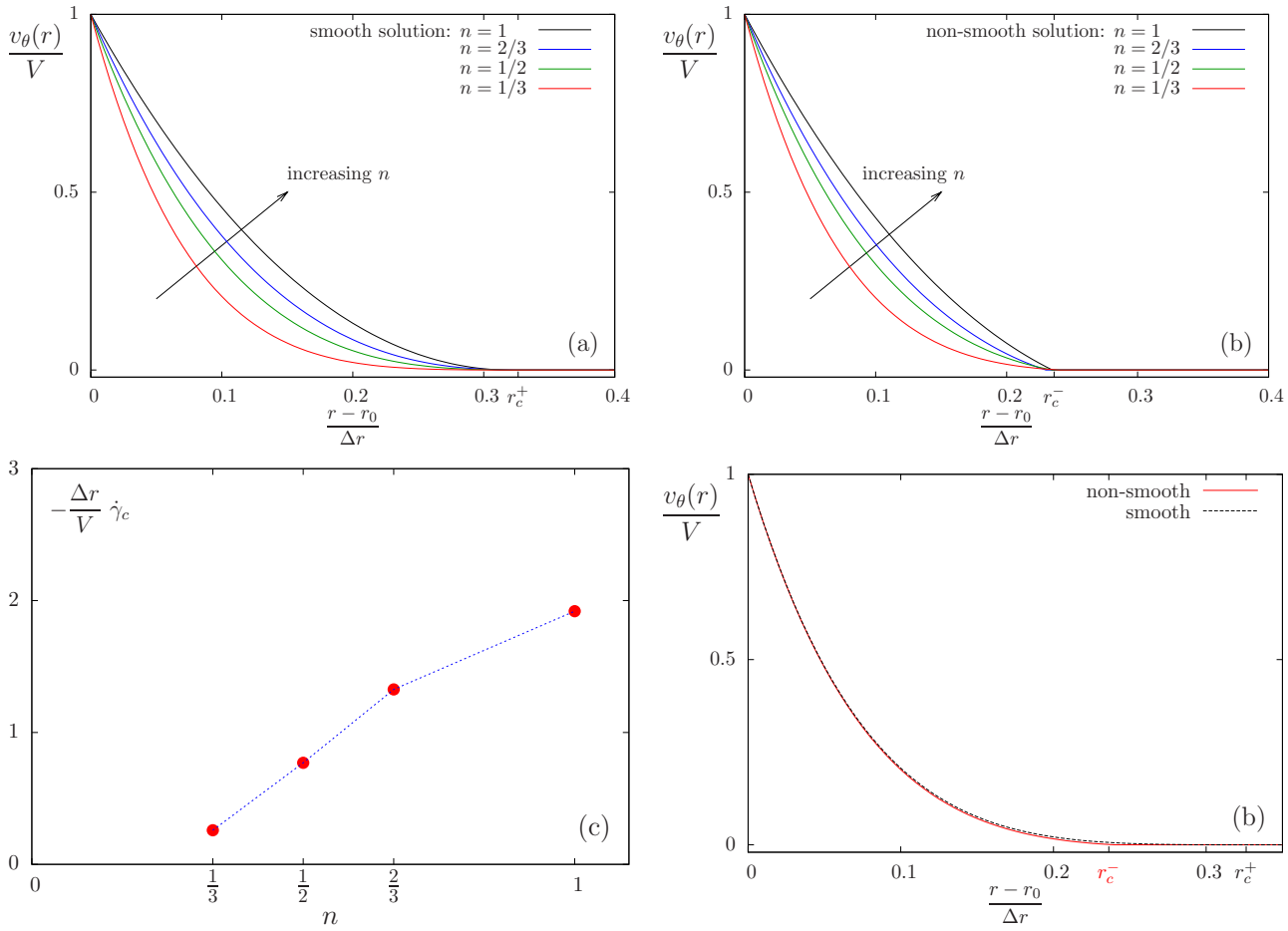


Figure 9: Effect of the shear thinning $n$ at fixed $r_c$: (a) smooth and (b) extreme non-smooth velocity profiles, (c) $\dot{\gamma}_c$ ; (d) smooth (dashed and black) and extreme non-smooth (continuous and red) profiles for $n = 1/3$.

Based on this procedure, the values of $n$ and $Bi$ are varying as in table 2 in such a way that $r_c$ remains constant. The solution is represented on Fig. 9. Fig. 9.a shows the smooth solution, associated to $r_c^+ \approx 0.3$ while Fig. 9.b plots the extreme non-smooth one, with $r_c^- \approx 0.23$. Note that now, both $r_c^+$ and $r_c^-$ are roughly constant. Observe that the velocity profile is more curved when $n$ is small. Fig. 9.c represents $\dot{\gamma}_c$: observe also that the discontinuity decreases rapidly for small $n$ values. For $n = 1/3$, the non-smoothness becomes imperceptible, while the smooth and extreme non-smooth profiles are very close and almost undiscernable, as shown on the insert of Fig. 9.d. Note that, even when $n = 1/3$, there are still multiple solutions, and the range for $r_c$ remains $[r_c^-, r_c^+] \approx [0.23, 0.3]$, despite the fact that these solution share very similar curved profiles.

# 4 Discussion

With these results, we can now revisit several debates on Couette flows, mentioned in the introduction.

## 4.1 Smooth and non-smooth profiles

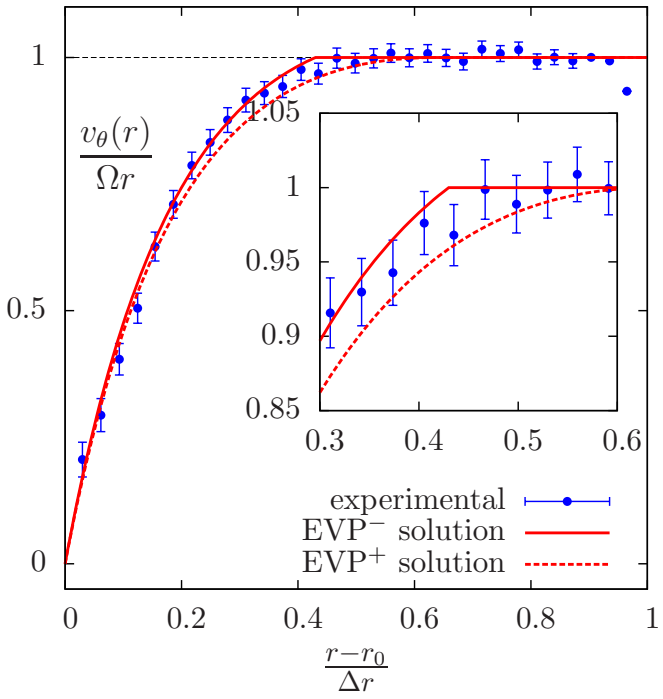


Figure 10: Foam with abrupt profile. Comparison of experimental data, from (Gilbreth et al., 2006), Fig 1, with model ($\varepsilon_Y = 0.2$, $Bi = 1.3$, $Co = 0.63333$, $n = 1$, $\alpha = 0.2$) for both extreme solutions: smooth EVP$^+$ and non-smooth EVP$^-$ ($\tau_{\theta\theta}(t{=}0) = \pm\sqrt{2}Bi$).

The debate between smooth and non-smooth velocity profiles is difficult to address experimentally, for two reasons.

First, since the stationary solution is not unique, both smooth and non-smooth profiles can be observed in the *same* experiment. This depends on the residual stresses due to initial preparation, which are usually not reproducible, and are certainly difficult to suppress (Raufaste et al., 2010). That could explain the doubts expressed by one author regarding the different results found at a few years interval, as reported on Fig. 1.b by Ovarlez et al. (2010).

Second, the experiments in foams are not always precise enough to discriminate between smooth and abrupt transitions. Fig. 10 compares experimental measurements and the two extreme solutions: $\text{EVP}^+$, the smooth one, with dashed lines, and $\text{EVP}^-$, the extreme non-smooth one, with solid lines. Experiments were performed with bubble rafts, and in order to reflect the absence of top and bottom plates, the fluid viscosity is introduced as a second Newtonian viscosity $\eta_2$ with a viscosity ratio $\alpha = \eta/(\eta + \eta_2)$ (see Saramito (2007, 2009)). In that case, the smooth solution predicts $r_c^+ = r_0 + 0.65\Delta r$ and the non-smooth one $r_c^- = r_0 + 0.43\Delta r$ together with a discontinuous shear rate $\dot{\gamma}_c = 0.33(V/\Delta r)$. Observe that both smooth and non-smooth solutions compare well with experimental measurements.

### 4.2 Is Couette flow suitable for EVP materials ?

Couette flows, due to their simple geometry, have a long history to probe the rheology of several Newtonian liquids. They are also very suitable to probe complex liquids such as VE or VP materials. However, the present study questions their use in EVP materials, and especially in foams, which are usually excellent models to perform in-lab experiments. In fact, in EVP materials, the initial conditions and the preparation method create residual stresses which are difficult to remove, and affect the flow, which thus becomes non-unique and poorly controlled. Care is necessary to interpret the results.

We thus recommend to study flows where residual stresses do not affect the understanding and measurements. Other requirements should include well-defined boundary conditions; good separation of scale between the discrete units, the representative volume element (RVE) and the global flow scale; large variation of the control parameters such as velocity (and, in foams: liquid fraction, dispersity of bubble sizes). We have shown using experiments and models that a Stokes flow of foam (flow around an obstacle) meets these requirements (Cheddadi et al., 2011a).

## Conclusion

We model here the Couette flow of elastic, viscous, plastic materials. We provide an approximate expression of the rheology versus different material parameters. These parameters are defined and measured at a mesoscopic scale, larger than discrete units, but smaller than the flow scale. These are experimentally measurable such as viscosity $\eta$ or the consistency $K$, the elastic modulus $\mu$ and yield strain $\tau_Y$. In turn, our predictions are compared with experiments. We have shown that there is a complex interplay between elasticity, viscosity and plasticity, which together (but not separately) account for experimental observations. We have also evidenced that even in such a simple geometry, the orientational effects are important, so that a tensor (rather than scalar) description is necessary to capture many

aspects of the physics.

The existence of localization in complex fluids can be predicted by the simple VP model. It is related with the heterogeneity of stress (whatever its cause, for instance the curvature of flow lines, or external friction): what matters is that the stress is either above or below the yield stress $\tau_Y$. In a localized flow, there are two distinct zones. Above $\tau_Y$, the material flows, below $\tau_Y$, the material remains rigid.

However, most subtle features, such as the effect of initial stresses conditions on the determination of either a smooth or a non-smooth profile, are due to the combined effect of the plasticity (the yield stress $\tau_Y$) and the elasticity $\mu$. The prediction of such features requires an EVP model, for which the previous mechanism is qualitatively modified: above $\tau_Y$, the material flows, , and the initial conditions are quickly erased by irreversible plastic deformations. Conversely, below $\tau_Y$, the material remains solid and elastic, with bounded deformations influenced by the initial stress conditions. The existence of normal stresses, the persistence of residual stresses, even in stationary flow, and apparition of non-smooth solutions in some situations can be predicted neither by VP models nor by VE models. The non-uniqueness of the stationary flow is a consequence of the combined effect of plasticity and elasticity in the fluid model.

We have computed numerically the value of the localization length versus different parameters: it mainly depends on viscoplastic effects (the dimensionless Bingham number). Non-smooth profiles are related to the appearance of a critical shear rate $\dot{\gamma}_c$. The effect of the initial conditions are more visible for instance when $\varepsilon_Y$ is large; or when the dissipation exponent $n$ is large; or when the velocity is large, but small enough to allow for a localization within the gap; or when the heterogeneity from the geometry is small, but large enough to allow for a localization within the gap.

Together, our results provide a validation of the continuous material description, a determination of EVP material parameters, and a in-depth understanding of their complex rheology. We have established several quantitatively testable predictions, regarding the values of localization length $r_c$ and critical shear rates $\dot{\gamma}_c$ (eq. 6). We have tested them against available experimental data, but many more tests are feasible. Moreover, it should be possible to test experimentally or numerically our main qualitative prediction: namely that initial conditions affect the flow, and even modify the continuous or discontinuous nature of the localization. Finally, it appears that the stationary Couette flow, which has stimulated so many debates, is not robust nor unique. Despite its apparent simplicity, it involves numerous parameters, such as initial stress tensor conditions, and is difficult to use in practice. We suggest that flows with a stronger dependence in time and/or space will provide much easier comparisons with simulations and models, and more stringent tests.

# Acknowledgments

We warmly thank M. Dennin and E. Janiaud for providing data, and B. Dollet for discussions. We than the french Groupe de Recherches "Mousses et Emulsions", C. Gay and C. Philippe-Barache for funding the travels for collaborations. FG thanks D. Weaire for intense discussions and questions which stimulated this work.

# References


J. D. Barry, D. Weaire, and S. Hutzler. Nonlocal effects in the continuum theory of shear localisation in 2d foams. *Phil. Mag. Lett.*, 91(6):432–440, 2011. URL `http://www.tara.tcd.ie/jspui/bitstream/2262/41088/1/The%20continuum%20theory.pdf`.

J.-F. Berret, D. C. Roux, and G. Porte. Isotropic-to-nematic transition in wormlike micelles under shear. *Europ. Phys. Journal E*, 4:1261–1279, 1994. URL `http://hal.archives-ouvertes.fr/docs/00/24/80/41/PDF/ajp-jp2v4p1261.pdf`.

E. C. Bingham. *Fluidity and plasticity*. Mc Graw-Hill, New-York, USA, 1922. URL `thttp://www.archive.org/download/fluidityandplast007721mbp/fluidityandplast007721mbp.pdf`.

I. Cantat, S. Cohen-Addad, F. Elias, F. Graner, R. Höhler, O. Pitois, F. Rouyer, and A. Saint-Jalmes. *Les mousses: structure et dynamique*. Belin, Paris, 2010.

I. Cheddadi, P. Saramito, C. Raufaste, P. Marmottant, and F. Graner. Numerical modelling of foam Couette flows. *Eur. Phys. J. E*, 27(2):123–133, 2008. URL `http://www-ljk.imag.fr/membres/Pierre.Saramito/epje.pdf`.

I. Cheddadi, P. Saramito, C. Raufaste, P. Marmottant, and F. Graner. Erratum to numerical modelling of foam Couette flows. *Eur. Phys. J. E*, 28:479–480, 2009. URL `http://www-ljk.imag.fr/membres/Pierre.Saramito/epje-erratum.pdf`.

I. Cheddadi, P. Saramito, B. Dollet, C. Raufaste, and F. Graner. Understanding and predicting viscous, elastic, plastic flows. *Eur. Phys. J. E. Soft matter*, 34(1):11001, 2011a. URL `http://www-ljk.imag.fr/membres/Pierre.Saramito/obstacle_evp.pdf`.

I. Cheddadi, P. Saramito, and F. Graner. Stationary Couette flows of elastoviscoplastic fluids, 2011b. http://www-roc.inria.fr/bang/IC/CheSarGra2011-supp-info.pdf.

R. J. Clancy, E. Janiaud, D. Weaire, and S. Hutzler. The response of 2D foams to continuous applied shear in a Couette rheometer. *Eur. Phys. J. E*, 21:123–132, 2006.

P. Coussot and G. Ovarlez. Physical origin of shear-banding in jammed systems. *Eur. Phys. J. E*, 33(3):183–188, 2010. URL `https://arxiv.org/pdf/1007.5479`.

P. Coussot, J. S. Raynaud, F. Bertrand, P. Moucheront, J. P. Guilbaud, H. T. Huynh, S. Jarny, and D. Lesueur. Coexistence of liquid and solid phases in flowing soft-glassy materials. *Phys. Rev. Lett.*, 88(21):218301, 2002.

F. da Cruz, F. Chevoir, D. Bonn, and P. Coussot. Viscosity bifurcation in granular materials, foams, and emulsion. *Phys. Rev. E*, 66:051305, 2002. URL `http://perso.lcpc.fr/chevoir.francois/P14.pdf`.

G. Debrégeas, H. Tabuteau, and J.-M di Meglio. Deformation and flow of a two-dimensional foam under continuous shear. *Phys. Rev. Lett.*, 87:178305, 2001. URL `http://arxiv.org/pdf/cond-mat/0103440`.

J. P. Decruppe, S. Lerouge, and J.-F. Berret. Insight in shear banding under transient flow. *Phys. Rev. E*, 63:022501, 2001.

N. D. Denkov, S. Tcholakova, K. Golemanov, and A. Lips. Jamming in sheared foams and emulsions, explained by critical instability of the films between neighboring bubbles and drops. *Phys. Rev. Lett.*, 103:118302, 2009. URL `http://arxiv.org/pdf/0901.3634`.

M. Dennin. Discontinuous jamming transitions in soft materials: coexistence of flowing and jammed states. *J. Phys.: Condens. Matter*, 20(2):283103, 2008. URL `http://arxiv.org/pdf/0801.2437`.

C. Gilbreth, S. Sullivan, and M. Dennin. Flow transition in two-dimensional foams. *Phys. Rev. E*, 74:031401, 2006. URL `http://www.physics.uci.edu/~dennin/preprints/gsd06.pdf`.

W. H. Herschel and T. Bulkley. Measurement of consistency as applied to rubber-benzene solutions. *Proceedings of the American Society for Testing and Material*, 26(2):621–633, 1926.

R. Höhler and S. Cohen-Addad. Rheology of liquid foam. *J. Phys. Condens. Matt.*, 17(41): R1041, 2005.

D. Howell, R. P. Behringer, and C. Veje. Stress fluctuations in a 2D granular Couette experiment: a continuous transition. *Phys. Rev. Lett.*, 82:5241–5244, 1999. URL `http://www.physics.emory.edu/~weeks/lab/papers/howell-prl99.pdf`.

N. Huang, G. Ovarlez, F. Bertrand, S. Rodts, P. Coussot, and D. Bonn. Flow of wet granular materials. *Phys. Rev. Lett.*, 94:028301, 2005. URL `http://arxiv.org/pdf/cond-mat/0412337`.

E. Janiaud and F. Graner. Foam in a two-dimensional Couette shear: a local measurement of bubble deformation. *J. Fluid Mech.*, 532:243–267, 2005.

E. Janiaud, D. Weaire, and S. Hutzler. Two-dimensional foam rheology with viscous drag. *Phys. Rev. Lett.*, 97:038302, 2006.

A. Kabla. *Plasticité et désordre dans les milieux divisés : mousses et matériaux granulaires.* PhD thesis, Université D. Diderot, Paris VII, 2003.

A. Kabla, J. Scheibert, and G. Debrégeas. Quasistatic rheology of foams I. Oscillating strain. *J. Fluid Mech.*, 587:23–44, 2007.

G. Katgert, M. E. Möbius, and M. van Hecke. Rate dependence and role of disorder in linearly sheared two-dimensional foams. *Phys. Rev. Lett.*, 101:058301, 2008. URL http://arxiv.org/pdf/0711.4024.

G. Katgert, A. Latka, M. E. Möbius, and M. van Hecke. Flow in linearly sheared two-dimensional foams: From bubble to bulk scale. *Phys. Rev. E*, 79(6):066318, 2009. URL http://arxiv.org/pdf/0903.5349.

G. Katgert, B. P. Tighe, M. E. Mobius, and M. M. van Hecke. Couette flow of two-dimensional foams. *Europhys. Lett.*, 90(5):54002, 2010. URL http://www.lorentz.leidenuniv.nl/~btighe/eplcouette.pdf.

S. A. Khan, C. A. Schnepper, and R. C. Armstrong. Foam rheology: III. Measurement of shear flow properties. *J. Rheol.*, 32:69–92, 1988.

K. Krishan and M. Dennin. Viscous shear banding in foam. *Phys. Rev. E*, 78:051504, 2008. URL http://arxiv.org/pdf/0806.3313.

J. Lauridsen, G. Chanan, and M. Dennin. Velocity profiles in slowly sheared bubble rafts. *Phys. Rev. Lett.*, 93(1):018303, 2004. URL http://www.physics.uci.edu/~dennin/preprints/lcd03preprint.pdf.

W. Losert, L. Bocquet, T. C. Lubensky, and J. P. Gollub. Particle dynamics in sheared granular matter. *Phys. Rev. Lett.*, 85:1428–1431, 2000. URL http://arxiv.org/pdf/cond-mat/0004401.

P. Marmottant, C. Raufaste, and F. Graner. Discrete rearranging disordered patterns, part II: 2D plasticity, elasticity and flow of a foam. *Eur. Phys. J. E*, 25:371–384, 2008. URL http://hal.inria.fr/docs/00/21/34/36/PDF/marmottant_T1.pdf.

D. M. Mueth, G. F. Debregeas, G. S. Karczmar, P. J. Eng, S. R. Nagel, and H. M. Jaeger. Signatures of granular microstructure in dense shear flows. *Nature*, 406:385–389, 2000. URL http://arxiv.org/pdf/cond-mat/0003433.

T. Okuzono and K. Kawasaki. Intermittent flow behavior of random foams: a computer experiment on foam rheology. *Phys. Rev. E*, 51:1246–1253, 1995.

J. G. Oldroyd. A rational formulation of the equations of plastic flow for a Bingham fluid. *Proc. Cambridge Philos. Soc.*, 43:100–105, 1947.

J. G. Oldroyd. On the formulation of rheological equations of states. *Proc. Roy. Soc. London A*, 200:523–541, 1950. URL http://rspa.royalsocietypublishing.org/content/200/1063/523.full.pdf#page=1&view=FitH.

G. Ovarlez, K. Krishan, and S. Cohen-Addad. Investigation of shear banding in three-dimensional foams. *Europhys. Lett.*, 91:68005, 2010. URL http://arxiv.org/pdf/1007.4133.

G. Porte, J.-F. Berret, and J. Harden. Inhomogeneous flows of complex fluids: mechanical instability versus non-equilibrium phase transition. *Eur. Phys. J. E*, 7:459–472, 1997. URL http://hal.archives-ouvertes.fr/docs/00/24/84/56/PDF/ajp-jp2v7p459.pdf.

C. Raufaste, S. J. Cox, P. Marmottant, and F. Graner. Discrete rearranging disordered patterns: prediction of elastic and plastic behavior, and application to two-dimensional foams. *Phys. Rev. E*, 81:031404, 2010. URL http://arxiv.org/pdf/1002.0732.

S. Rodts, J. C. Baudez, and P. Coussot. From discrete to continuum flow in foams. *Europhys. Lett.*, 69(4):636–642, 2005. URL http://www.physics.emory.edu/faculty/weeks/lab/papers/coussot-epl05.pdf.

J.-B. Salmon, A. Colin, S. Manneville, and F. Molino. Velocity profiles in shear-banding wormlike micelles. *Phys. Rev. Lett.*, 90:228303, 2003a. URL http://arxiv.org/pdf/cond-mat/0211475.

J.-B. Salmon, S. Manneville, and A. Colin. Shear banding in a lyotropic lamellar phase. ii. temporal fluctuations. *Phys. Rev. E*, 68:051504, 2003b. URL http://arxiv.org/pdf/cond-mat/0307609.

P. Saramito. A new constitutive equation for elastoviscoplastic fluid flows. *J. Non Newtonian Fluid Mech.*, 145(1):1–14, 2007. URL http://www-ljk.imag.fr/membres/Pierre.Saramito/evp.pdf.

P. Saramito. A new elastoviscoplastic model based on the Herschel-Bulkley viscoplasticity. *J. Non Newtonian Fluid Mech.*, 158(1–3):154–161, 2009. URL http://www-ljk.imag.fr/membres/Pierre.Saramito/evp-hb.pdf.

P. Saramito. *Efficient C++ finite element computing with Rheolef.* CNRS and LJK, 2011. URL http://www-ljk.imag.fr/membres/Pierre.Saramito/rheolef/rheolef.pdf. http://www-ljk.imag.fr/membres/Pierre.Saramito/rheolef/rheolef.pdf.

P. Schall and M. van Hecke. Shear bands in matter with granularity. *Annu. Rev. Fluid Mech.*, 42:67–88, 2010. URL http://www.physics.leidenuniv.nl/sections/cm/grm/articles/ANRV400-FL42-04%255B067-088%255D.pdf.

Y. Wang, K. Krishan, and M. Dennin. Impact of boundaries on velocity profiles in bubble rafts. *Phys. Rev. E*, 73:031401, 2006. URL http://www.physics.uci.edu/~dennin/preprints/wkd05a.pdf.

D. Weaire and S. Hutzler. *The physics of foam.* Oxford University Press, UK, 1999.

D. Weaire, J. D. Barry, and S. Hutzler. The continuum theory of shear localization in two-dimensional foam. *J. Phys.: Condens. Matter*, 22:193101, 2010. URL http://www.tara.tcd.ie/bitstream/2262/41088/1/The%20continuum%20theory.pdf.

# A Equations in cylindrical geometry

The velocity field is $\mathbf{v} = (0, v_\theta, 0)$ in cylindrical $(r, \theta, z)$ coordinates. The elastoviscoplastic constitutive equation in cylindrical coordinates writes:

$$\frac{1}{2\mu}\frac{\partial \tau_{rr}}{\partial t} + \max\left(0, \frac{|\boldsymbol{\tau}_d| - \tau_Y}{2K|\boldsymbol{\tau}_d|^n}\right)^{\frac{1}{n}} \tau_{rr} = 0, \tag{7}$$

$$\frac{1}{2\mu}\left(\frac{\partial \tau_{r\theta}}{\partial t} - 2D_{r\theta}\tau_{rr}\right) + \max\left(0, \frac{|\boldsymbol{\tau}_d| - \tau_Y}{2K|\boldsymbol{\tau}_d|^n}\right)^{\frac{1}{n}} \tau_{r\theta} = D_{r\theta}, \tag{8}$$

$$\frac{1}{2\mu}\left(\frac{\partial \tau_{\theta\theta}}{\partial t} - 4D_{r\theta}\tau_{r\theta}\right) + \max\left(0, \frac{|\boldsymbol{\tau}_d| - \tau_Y}{2K|\boldsymbol{\tau}_d|^n}\right)^{\frac{1}{n}} \tau_{\theta\theta} = 0,, \tag{9}$$

with $|\boldsymbol{\tau}_d| = \left(2\tau_{r\theta}^2 + \frac{1}{2}(\tau_{rr} - \tau_{\theta\theta})^2\right)^{1/2}$. Here, $D = (\nabla\mathbf{v} + \nabla\mathbf{v}^T)/2$ is the rate of strain tenor, $K$ denotes a generalized viscosity (see Saramito (2009)). The conservation of momentum writes:

$$\frac{\partial p}{\partial r} - \frac{\partial \tau_{rr}}{\partial r} - \frac{\tau_{rr} - \tau_{\theta\theta}}{r} = 0, \tag{10}$$

$$-\frac{1}{r^2}\frac{\partial}{\partial r}\left(r^2\tau_{r\theta}\right) = 0 \tag{11}$$

This system of equations is closed by boundary conditions for the velocity at the inner and external cylinders, respectively $r = r_0$ and $r = r_e$, (see Fig. 1a) and by initial conditions for both the velocity $v_\theta$ and the elastic stress $\tau$.

# B Herschel-Bulkley solution in cylindrical geometry

When $\varepsilon_Y = 0$ the EVP model reduces to the VP one, and the velocity profile is given by

$$v_\theta(r) = \left(\frac{\sqrt{2}\, r_c^2\, \tau_Y}{K}\right)^{\frac{1}{n}} r \int_r^{r_c} \frac{1}{s}\left(\frac{1}{s^2} - \frac{1}{r_c^2}\right)^{\frac{1}{n}} \mathrm{d}s$$

In the case where the flow is driven by the inner boundary, the critical radius $r_c$ is given by the following expression:

$$\tau_Y = \frac{K}{\sqrt{2}\, r_c^2}\left(\frac{v(r_0)}{r_0 \displaystyle\int_{r_0}^{r_c} \frac{1}{s}\left(\frac{1}{s^2} - \frac{1}{r_c^2}\right)^{\frac{1}{n}} \mathrm{d}s}\right)^n.$$

It expresses also in dimensionless variables:

$$Bi = \sqrt{2}\left(\frac{\Delta r}{r_c}\right)^2 \left( \frac{1}{\dfrac{r_0}{\Delta r}\displaystyle\int_{r_0/\Delta r}^{r_c/\Delta r} \frac{1}{s}\left(\frac{1}{s^2} - \left(\frac{\Delta r}{r_c}\right)^2\right)^{\frac{1}{n}} \mathrm{d}s} \right)^n , \tag{12}$$

For fixed values of $n$ and $r_c$, the corresponding value of $Bi$ for the VP model, denoted as $Bi_{\mathrm{vp}}(n, r_c)$, can be easily computed by using numerical integration. Conversely, for given $Bi$ and $n$, the value of $r_c$ associated to the the VP model, denoted as $r_{c,\mathrm{vp}}(n, Bi)$, can be obtained from a small numerical computation (see Fig. 11a).

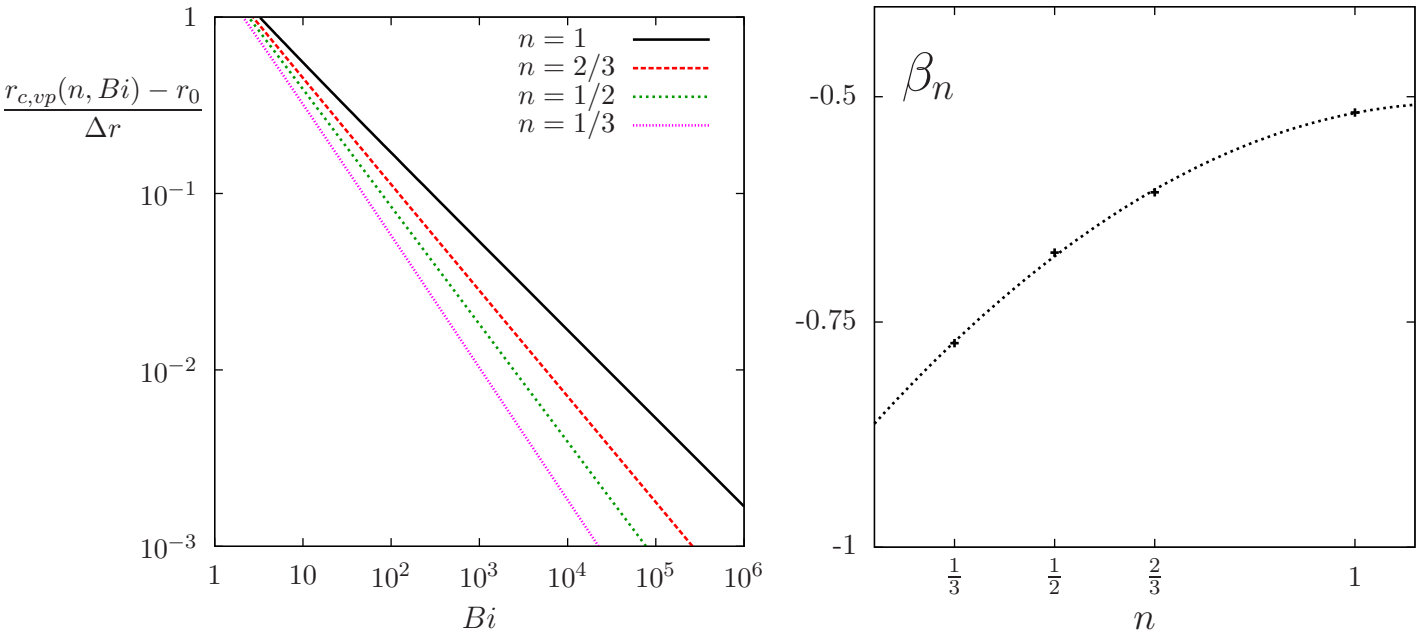


Figure 11: Herschel-Bulkley model ($\varepsilon_Y = 0$, $Co = 1/3$): (a) localization $r_c = r_{c,hb}(Bi, n)$ as a function of the Bingham number $Bi$, for different values of the power index $n$ ; (b) Index $\beta_n$ vs $n$ for the power law $(r_c(Bi, n) - r_0)/\Delta r \approx 1.82\, Bi^{\beta_n}$.

Fig. 11a plots $r_c$ as a function of the Bingham number $Bi$, for $\varepsilon_Y = 0$ (VP model) and $Co = 1/3$, and different values of the power index $n$. (see appendix B, equation (12) for this short computation). Note that the value $Co = 1/3$ corresponds to the geometry of the experiment by Coussot et al. (2002) as shown on Fig. 3b. In this geometry, the localization is observed as long as $r_c/\Delta r < r_e/\Delta r = 1/Co$. The VP model predicts that $r_c$ decreases with the Bingham number: the zero-velocity zone develops and the localization effect is more pronounced. Observe also that the localization effect is more pronounced when $n$ decreases at fixed values of $Bi$ and $Co$. The value $r_c$ value associated to the VP model is denoted as

$r_{c,\mathrm{vp}}(n, Bi)$ and this inverse at fixed $n$ as $Bi_{\mathrm{vp}}(n, r_c)$. Since $r_c$ depends roughly as a power law upon $Bi$ at fixed $n$, e.g. $(r_c(Bi, n) - r_0)/\Delta r \approx 1.82\, Bi^{\beta_n}$, Fig. 11b represents $\beta_n$ vs $n$. A nonlinear regression leads to $\beta_n \approx -0.38\, n^2 + 0.88\, n - 1.02$, represented as a dotted line.

# C Numerical method

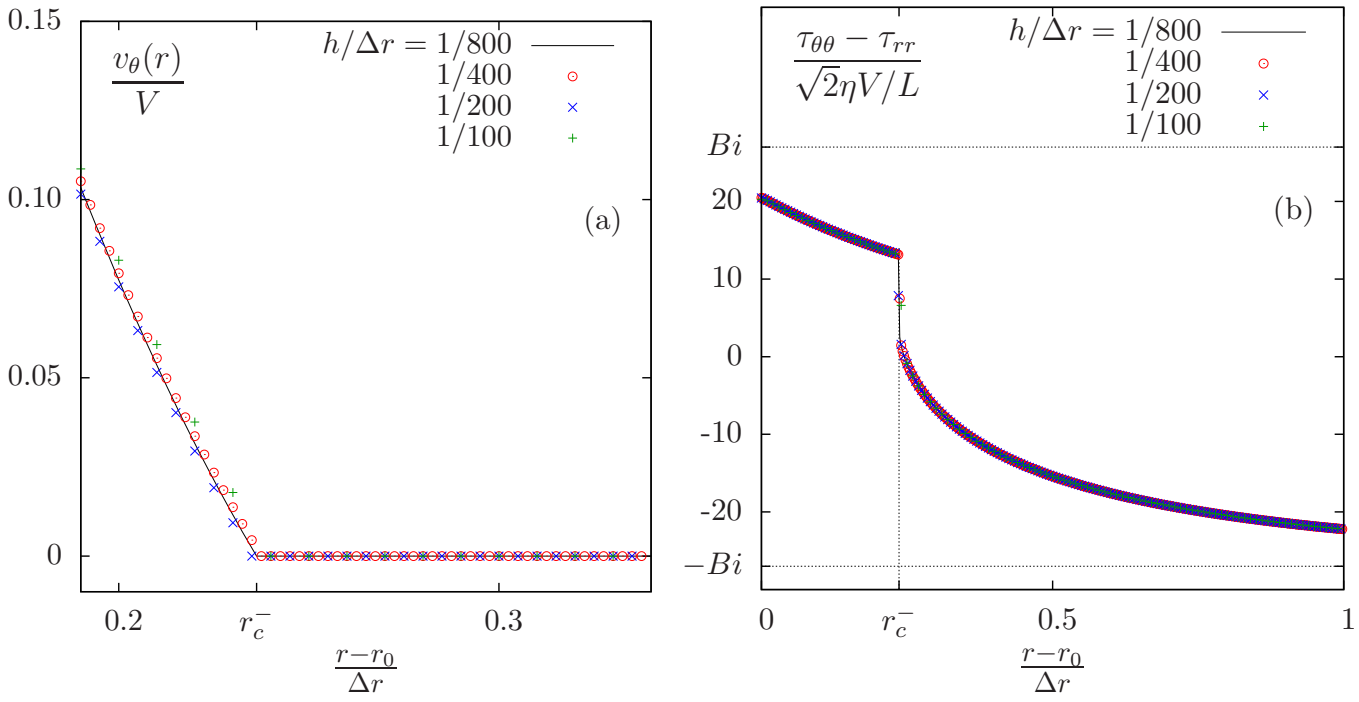


Figure 12: Convergence versus mesh refinement for the EVP$^-$ non-smooth solution ($\varepsilon_Y = 0.35$, $Bi = 27$, $Co = 1/3$, $n = 1$) as on Fig. 2.

The velocity is approximated by continuous affine finite elements while the stress components are piecewise constant over the mesh. The code is implemented by using the $C++$ Rheolef finite element library (Saramito, 2011). The stopping criteria for a stationary solution is satisfied when the residual term is less than $10^{-8}$. Fig. 12 shows the convergence versus the mesh size $h$ at the vicinity of $r = r_c$ for the EVP$^-$ non-smooth stationary solution presented on Fig. 2. Observe that the numerical method presents excellent convergence properties, despite the non-smoothness of the solution: the velocity is non-differentiable (Fig. 12a) while normal stress is discontinuous (Fig. 12b).